

Where do We Poop? City-Wide Simulation of Defecation Behavior for Wastewater-Based Epidemiology

HOSSEIN AMIRI, Emory University, USA

AKSHAY DEVERAKONDA, Emory University, USA

YUKE WANG, Emory University, USA

ANDREAS ZÜFLE, Emory University, USA

Wastewater surveillance, which regularly examines the pathogen biomarkers in wastewater samples, is a valuable tool for monitoring infectious diseases circulating in communities. Yet, most wastewater-based epidemiology methods, which use wastewater surveillance results for disease inferences, implicitly assume that individuals excrete only at their residential locations and that the population contribute to wastewater samples are static. These simplifying assumptions ignore daily mobility, social interactions, and heterogeneous toilet use behavior patterns, which can lead to biased interpretation of wastewater results, especially at upstream sampling locations such as neighborhoods, institutions, or buildings. Here, we introduce an agent-based geospatial simulation framework: Building on an established Patterns of Life model, we simulate daily human activities, mobility, and social contacts within a realistic urban environment and extend this agent-based framework with a physiologically motivated defecation cycle and toilet usage patterns. We couple this behavioral model with an infectious disease model to simulate transmissions through spatial and social interactions. When a defecation occurs for an infected agent, we use a pathogen shedding model to determine the amount of pathogen shed in the feces. Such a framework, integrating population mobility, disease transmission, toilet use behavior, and pathogen shedding models, is capable to simulate the Spatial-temporal dynamics of wastewater signals for a city. Using a case study of 10,000 simulated agents in Fulton County, Georgia, we examine how varying infection rates alter epidemic trajectories, pathogen loads in wastewater, and the spatial distribution of contamination across time. Our results highlight that mobility and toilet use can substantially decouple residential population counts from wastewater signals and demonstrate how behaviorally grounded simulations can support interpretation, scenario analysis, and the design of wastewater surveillance strategies.

Additional Key Words and Phrases: Patterns of Life, Simulation, Wastewater-Based Epidemiology, Defecation Behavior

1 Introduction

Wastewater surveillance (WWS) is a public health tool that regularly measures biomarkers in wastewater samples, including pooled samples of feces, urine, and sputum from the population using sewage systems, to monitor infectious disease prevalence in the community. Since the start of the COVID-19 pandemic, this novel approach has been widely implemented to supplement the use of epidemiological case surveillance for rapidly identifying disease outbreaks [30, 39], monitoring temporal and spatial trends in disease transmission [15, 38], and guiding disease prevention and control measures [14, 34].

Fig. 1 illustrates the Wastewater Surveillance process: (1) Assume we have a study region, such as a city, in which individuals carrying an infectious diseases live. In **Fig. 1**, we highlight homes and a hospital housing infectious agents in red color. People use the toilet and, depending on their disease status, release loads of pathogens into their local sewer system. The pathogens travel down-stream from local wastewater pipes of individual homes into the sewer network of the local neighborhood, into larger sewer network of increasingly larger neighborhoods until eventually reaching wastewater processing plants where wastewater is collected. (2) Wastewater surveillance extracts wastewater samples

Authors' Contact Information: Hossein Amiri, hossein.amiri@emory.edu, Emory University, Atlanta, USA; Akshay Deverakonda, Akshay.deverakonda@emory.edu, Emory University, Atlanta, USA; Yuke Wang, yuke.wang@emory.edu, Emory University, Atlanta, USA; Andreas Züfle, azufle@emory.edu, Emory University, Atlanta, USA.

Manuscript submitted to ACM

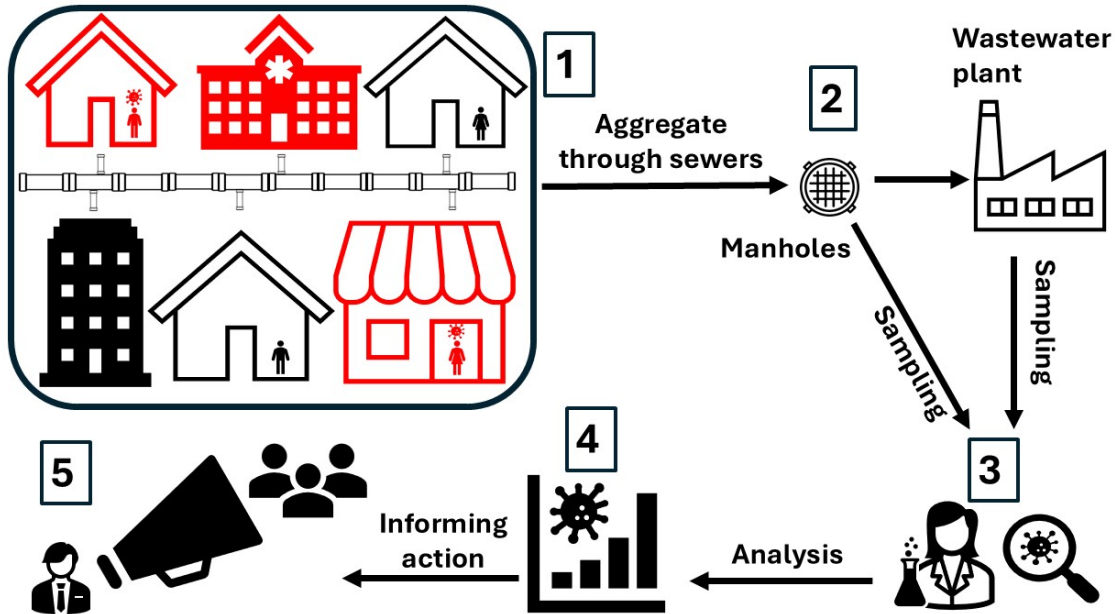


Fig. 1. Conceptual overview of wastewater surveillance. (1) In a specific geographic area covered by a sewer system, referred to as a sewershed, infected (in red) and non-infected (in black) persons from different buildings contribute fecal waste into a sewer system. (2) We can collect wastewater samples either from manholes located across the sewer system or at the downstream wastewater treatment plant. (3) We can analyze samples to detect the presence of pathogens and quantify their levels. (4 and 5) The wastewater surveillance results can help us estimate trends in pathogen prevalence over time in the sewershed, informing public health response.

*Sewer manhole icon used in this diagram obtained from Flaticon.com.

at any point in the sewer network: At the processing plant or at any point upstream from sewer manholes which may collect wastewater from communities, neighborhoods, or individual homes. (3) The collected samples are analyzed in labs to detect the load of a pathogen using highly sensitive testing. For example, for COVID-19, signals coming from as few as one infected person among tens of thousands can still be detected [13]. (4) These signals are analyzed for spatial and temporal trends, to identify local outbreaks, such as outbreaks at student residence halls at Emory University [39]. (5) Finally, these trends are communicated to policy makers such as leaders in university administration or state, indigenous, local, or territorial health departments to take preventative action such as informing residents, pre-emptive resource allocation, and protecting vulnerable communities.

For simplicity, most wastewater-based epidemiology (WBE) studies, which infer disease trends using wastewater data, assume that individuals only use toilets in their residential location [20, 32] without considering human mobility. Numerous recent WBE programs have been used for sentinel surveillance to monitor specific sites in dense urban areas (e.g., hospitals, university campuses, airports, conference centers, stadiums, and correctional facilities) [11, 12, 22, 28, 39]. Our hypothesis is that ignoring human mobility may underestimate disease prevalence in residential areas while overestimating it in commercial areas. For example, a commercial area having many workplaces but few residential houses would attribute all pathogens from many workers to a few residents. For instance, during the COVID-19 pandemic, shelter-in-place orders, which required all residents and visitors to remain in their residences and limit social

interactions, led to a decline in SARS-CoV-2 concentrations in wastewater samples from sites capturing commercial areas. This decrease reflected reduced population mobility rather than a decline in disease burden and highlights how biased estimations can complicate disease trend analysis and public health decision-making. Thus, we postulate that it is critical to consider human mobility rather than assuming home-only toilet use. Towards this, the goal of this study is to drop the assumption of only using toilets at home by using geosimulation to (1) simulate realistic spatial pooping behavior at the individual level, (2) simulate an infectious disease outbreak within the simulated populations and the corresponding release of pathogens (shedding) into the sewer network, and (3) share the simulation framework and generated example datasets to support WBE.

Recent studies have begun to integrate agent-based infection dynamics, human mobility, pathogen shedding, and wastewater transport within unified frameworks for wastewater-based epidemiology [10, 29]. However, existing models do not explicitly combine high-resolution individual-level population mobility, social contact patterns, toilet-use behavior (defecation events and toilet choice), and mechanistic within-host shedding dynamics in a single scalable agent-based geospatial simulation that is capable to generate the number of pathogens enters the sewer system through a toilet at a specific time. To the best of our knowledge, no current modeling framework integrates all of these components in the unified way proposed here. Connecting this model with models of pathogen fate in sewerage, WWS, and public health interventions will create a comprehensive “playground” for conducting scenario studies of disease transmission and assessing impact of public health interventions altering human behavior and reducing disease transmissions. In this paper, we address this gap by proposing an agent-based geospatial simulation that explicitly links human behavior, infectious disease dynamics, and wastewater signals. With these insights, our main contributions are as follows:

- We develop a geospatial simulation framework that integrates high resolution population mobility, social contact patterns, infectious disease transmission, toilet use behavior, and pathogen shedding dynamics into a single scalable model for generating wastewater system inputs.
- We extend the Patterns of Life simulation with a physiologically motivated defecation mechanism that drives agent level toilet choice across homes, workplaces, and public venues, which allows wastewater contributions to be attributed to both residents and travelers within each sewershed.
- We design an agent-based SEIR infection model with multi layer transmission through co location and social networks, heterogeneous progression times, and a gamma like within host shedding function that links respiratory transmission to fecal pathogen loads in wastewater.
- We demonstrate the framework in a case study of 10,000 agents in Fulton County, Georgia, USA, and show how mobility patterns, infection rates, and toilet use jointly shape epidemic curves, spatial spread of infection, and the temporal dynamics of pathogen loads that would be observed through wastewater based epidemiology.
- We publish the source code on an opensource project on GitHub (<https://github.com/onspatial/wastewater-based-epidemiology-patterns-of-life>)

The remainder of the paper is organized as follows. **Section 2** provides background on the wastewater surveillance, wastewater based epidemiology, and Patterns of Life simulation. **Section 3** reviews related work on dynamic populations in sewersheds, mobility informed wastewater analysis, and simulation based approaches. **Section 4** presents our methodology, including the extended behavioral dynamics, infectious disease and shedding models, and parameter settings. **Section 5** reports experimental results for the Fulton County case study, analyzing disease dynamics, pathogen loads, and spatial patterns of spread. **Section 6** discusses implications for interpreting wastewater signals and designing surveillance strategies. **Section 7** concludes and outlines directions for future research.

2 Background

In this section, we provide the background information, including an overview of WWS, WBE, and the Patterns of Life Simulation.

2.1 Wastewater surveillance

WWS is a public health monitoring approach that analyzes sewage samples to detect and track diseases or other health-related issues within a community. Unlike traditional epidemiological surveillance, which conducts individual-level clinical testing, WWS examines what entire populations collectively excrete into the sewer system, providing a community-level snapshot of health status. The concept has roots dating back to the mid-20th century when researchers successfully used wastewater to monitor poliovirus circulation in different geographic regions, demonstrating the feasibility of tracking infectious diseases through sewage systems [24, 27, 35].

The WWS process involves collecting wastewater from strategic sampling points in the sewerage system—typically at downstream treatment facilities or specific upstream locations—and analyzing these samples in the laboratory to detect genetic material or other biomarkers of interest. The resulting data can reveal patterns of disease presence and spread across communities served by the sewer system. This approach offers several compelling advantages for public health agencies. It provides population-level monitoring without requiring individual testing [34], can detect signals from both symptomatic and asymptomatic infections [20], and often serves as an early warning system for disease outbreaks [18, 39]. Additionally, WWS is generally more cost-effective than mass individual testing programs and can capture information from under-served populations that may not have adequate testing capacity.

2.2 Wastewater-based epidemiology

WBE, building upon the infrastructure of WWS, establishes a comprehensive framework to infer health outcomes from wastewater measurements. While WWS focuses primarily on detection and monitoring the presence of targeted biomarkers in wastewater, WBE represents a broader analytical approach that uses wastewater measurements to draw inferences about population health, behaviors, and exposures [25, 32]. Essentially, WBE treats wastewater as a pooled biological sample that captures the collective biochemical "fingerprint" of a community.

During the COVID-19 pandemic, WBE gained its popularity as research institutes/organizations and government agencies worldwide implemented WWS for SARS-CoV-2, demonstrating its value for tracking pandemic trends, identifying emerging hotspots, and providing early warnings of surges in infections—including at localized scales such as university campuses and residential facilities [15, 30, 38, 39]. The scope of WBE encompasses diverse applications beyond infectious disease monitoring. Researchers have used this approach to track pharmaceutical consumption, estimate illicit drug use, assess nutritional status through metabolic markers, and monitor environmental chemical exposures at the population level [7, 23].

The primary strength of WBE lies in its objectivity and near-real-time nature, as it captures unbiased population-level data independent of healthcare-seeking behavior or testing availability. It can reveal trends in hard-to-reach populations and detect asymptomatic infections that would otherwise go unnoticed in epidemiological surveillance systems [20]. However, WBE also has important limitations. The data represents aggregated community-level information rather than individual cases, making it impossible to identify specific infected persons or their precise locations within a sewer catchment area [38]. Additionally, the relationship between wastewater signals and actual disease prevalence can

be influenced by factors such as pathogen shedding variability among infected individuals, wastewater dilution, and environmental degradation of target biomarkers, toilet use behavior, and population mobility [20, 32, 37].

2.3 Patterns of Life Simulation

The pattern-of-life simulation [42] used in this study is an established agent-based framework that captures a broad range of human behaviors, including working, staying at home, sleeping, eating, and interacting with friends and strangers at public spaces such restaurants and recreational sites. The framework is theory-driven, with behavioral logic grounded in established models of human activity. In particular, agents make decisions based on their needs, structured around Maslow's hierarchy of needs [19], encompassing physiological requirements (food, shelter, sleep), safety needs (financial safety), and social needs (love). Meeting these needs enables agents to sustain homeostasis and overall well-being. The design and validation of this framework have been thoroughly documented in prior studies [1, 16]. The simulation has been used as a baseline framework for data generation and has been extended with additional features, including anomalous agents and infectious disease modeling [2, 3, 17, 40, 41].

The Patterns of Life simulation represents everyday human activity within real geographic environments, or within synthetically generated maps created for specific purposes such as fictional cities. Time progresses in discrete steps mapped to real clock time, allowing the model to track hours, days, weekdays and weekends, as well as calendar events such as national holidays, while agents live in homes, work, eat out, and socialize. The simulated world can be initialized using real map layers containing buildings, building units, and walkways. The city is divided into neighborhoods, with each building assigned a functional type and an attractiveness score. Spatial layers are aligned to support agent mobility through a routing network capable of distance and nearest-place queries. More specifically, the map is retrieved from OpenStreetMap. Buildings and building units are extracted separately, and walkways and paths are captured in a dedicated file to serve as simulation inputs. The simulation requires three map files, each carrying specific information: the *buildings.shp* file contains building footprints, the *buildingUnits.shp* file stores building unit attributes, and the *walkways.shp* file defines the transportation network. Within each neighborhood, the model generates apartments, workplaces with jobs and schedules, classrooms in schools, restaurants, and recreational places. Capacities, costs, and attractiveness values are sampled from specified distributions and neighborhood composition rules, ensuring that the simulated built environment reflects realistic local mixes of residential, commercial, and educational sites. The population includes single individuals and families distributed across neighborhoods. Each agent is assigned demographic and behavioral attributes such as age, education, interests, finances, movement speed, food needs, and social requirements.

The simulation explicitly models daily rhythms. At midnight, global updates process rent, tuition, aging, financial balances, and reset daily counters. Evening routines update social well-being and generate plans for the following day. Nightly summaries compute venue visitation profiles, apply decay to social ties, prune weak relationships, and calculate the expected strength of stable connections. Agents follow daily plans balancing home, work, meals, and recreation, moving along the walkway network and selecting destinations such as restaurants and pubs based on network distance and environmental conditions. Two directed social graphs are maintained: one representing family and friendship networks, and another capturing work relationships. Social interactions strengthen ties, while inactivity causes ties to decay; links that fall below a threshold are removed. These evolving networks can be visualized in real time or exported for post-simulation analysis. Economic behavior is also incorporated: agents earn income through jobs that vary by education requirements, pay rates, schedules, and workdays, while incurring expenses such as housing and

tuition. Financial balances are dynamically updated as earnings and expenditures accumulate, providing a realistic representation of individual and household economics within the simulated urban system.

3 Related Works

3.1 Measures of dynamic populations in sewersheds

In wastewater surveillance, population normalization enables the comparison of wastewater measurements from the same sampling location across different timepoints and from different sampling locations. However, estimating the catchment population size to use for normalization has various degrees of uncertainty, depending on the methodology used [9].

Currently, there are two common methodologies for normalizing catchment populations. First method is using census data, whose advantage is that these data are relatively accessible and are inexpensive if not free to access [26]. One study in France studied the relation between wastewater flow rate and mobility into and out of a catchment area, as determined from census surveys [5]. The study found that changes in mobility correlated to changes in certain pollutants over the study period. Another study used census data to estimate population sizes in catchment areas, and found that they were different than the reported population numbers from WWTPs [36]. An advantage of using census data is that it is accompanied by sociodemographic data such as income levels, age, etc. that can be applied to the catchment area [9]. A disadvantage to using census data is that methods used involving it for population normalization in wastewater surveillance are not usually reported in the literature, and different methods can result in wildly different population estimates [26]. Additionally, wastewater catchment areas may not overlap perfectly with census tracts [9].

3.2 Mobility and wastewater data

One niche of estimating dynamic populations in wastewater surveillance has been using mobile-device data and/or other forms of signaling data. An advantage of using mobile device data compared to biomarkers is that it can contain info on real-time movements of people possessing phones [6, 33]. Thomas et al. 2017 was one of the first studies to use mobile device data to show that the population within a catchment area varied over multiple timescales ranging from within a day to across a month. They used this variability to calculate population normalized loads of illicit drugs that accounted for dynamic populations over the study period. Another study used mobile device data to improve understanding of psychoactive pharmaceutical use in a catchment area over two years [8]. Integrating mobility data into this study's analysis helped improve the interpretability of pharmaceutical usage due to having a better understanding of how the underlying population size changed over time.

In addition to examining population-normalized loads of substances/pollutants, authors have used mobility data to characterize wastewater flows. Researchers from one study assessed correlations between mobility data and wastewater flows across five catchment areas in Sweden, and their results showed promise for further investigation using more refined modeling techniques [21].

A drawback to using mobility data is its expensiveness and the need for an advanced skillset to be able to work with it. One study, however, showed ammonium correlates with mobility and can be a proxy for normalizing population changes in a catchment area [6]. Another study compared daily loads of methamphetamine that were population normalized according to mobile device data, total nitrogen, total phosphorus, biological oxygen demand, and census data, and found that mobile-device data was much better than the other data sources at estimating real-time population changes, and especially so in a specific catchment area rather than an entire metropolitan area [31].

Table 1. Behavioral and physiological needs represented in the pattern of life simulation, compared to the existing simulation (Vanilla).

	Food	Love	Shelter	Sleep	Financial Safety	Defecation	Infection Diseases
This Version	✓	✓	✓	✓	✓	✓	✓
Vanilla Version	✓	✓	✓	✓	✓	✗	✗

3.3 Simulating dynamic populations in wastewater sewersheds

While there are many different methods in the literature for characterizing dynamic populations in sewersheds, these measures of fluctuation are centered around change in the population in the sewershed over time. Fewer studies have examined the spatial variation in dynamic populations to examine how their distribution changes over space, and especially how this spatial variation changes across time. One previous study constructed an agent-based model to simulate wastewater production, especially by infected agents during a simulated disease outbreak [10].

4 Methodology

In this section, we provide the methodology including the simulation dynamics that capture daily and weekly human behavioral patterns in five-minute resolution, the infectious disease modeling framework governing transmission and recovery, the mechanistic representation of defecation events contributing to wastewater, the modeling of pathogen growth and decay within the sewer network, and the analytical methods used for data processing and interpretation.

4.1 Simulation of Defecation Behavior

The Patterns of Life Simulation [1, 42] is an agent-based framework grounded in physiological and sociological mechanisms inspired by Maslow’s theory of human needs[19]. In this framework, an agent’s behavior is guided by its underlying needs, which drive decision making and daily activity patterns. The baseline model includes essential needs such as food, love, sleep, shelter, and financial safety, which together drive individual activities and social interactions. Following the same design principle, we introduce an additional physiological element to represent the defecation need, allowing agents to exhibit more natural and biologically consistent behavior. A comparison of the baseline model and the extended model presented in this paper is provided in **Table 1**. As shown, our updated framework introduces two additional components—defecation and infectious disease dynamics—that were not included in the vanilla version. These additions allow the simulation to capture more realistic behavioral and Wastewater-based Epidemiology related patterns observed in populations.

In the extended simulation framework, we introduce a new physiological mechanism captures the gradual buildup and relief of a biological need over time. Each agent continuously tracks its internal state, as shown in **Fig. 2**, which evolves based on elapsed time and an individual characteristic called the defecation rate, drawn from a uniform distribution. The process progresses through multiple stages, ranging from complete comfort to increasing urgency, depending on how much time has passed since the last relief event. These transitions are governed by specific thresholds that determine when an agent experiences mild, moderate, or urgent pressure. Once the need is satisfied, the internal state resets, initiating a new cycle. This continuous time-dependent regulation strengthens the model’s temporal consistency and introduces a natural rhythm into agent behavior.

After each relief event, the agent experiences a comfortable period that gradually transitions into rising internal pressure as simulated time passes. The rate of this buildup varies among agents, reflecting individual-level heterogeneity in biological rhythms, and daily routines. When the internal pressure surpasses a defined threshold, the agent becomes

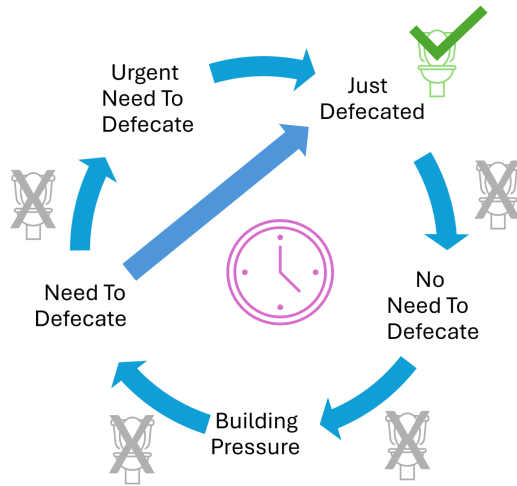


Fig. 2. Defecation cycle within the simulation. The process begins with the '*Just Defecated*' state and progresses through subsequent stages before returning to the start. The full cycle may repeat multiple times per day, depending on each agent's individual defecation rate.

increasingly aware of the need and eventually must take action to relieve it. The agent will only take this action when not in transit; for instance, while at home, work, or in a public location. These transitions are smooth and progressive rather than abrupt, enabling the simulation to represent realistic behavioral variability. Integrating this physiological mechanism within the broader hierarchy of needs allows the simulation to represent a more holistic view of human behavior. As internal pressure increases, agents may alter their plans or temporarily re-prioritize tasks to address their bodily needs, just as people do in real life. This dynamic interplay between biological, social, and environmental drivers generates emergent behavioral patterns that evolve naturally across the population. Differences in individual timing and urgency create realistic variations in activity peaks, movement density, and location demand.

More specifically, Fig. 2 illustrates a five-state progression: '*Just Defecated*' → '*No Need To Defecate*' → '*Building Pressure*' → '*Need To Defecate*' → '*Urgent Need To Defecate*'. At initialization, each agent is assigned a defecation rate sampled from a uniform distribution to capture inter-individual variability. This rate sets three timing controls: how long it takes to leave '*No Need To Defecate*', how long that comfort is maintained, and how quickly internal pressure builds per simulation step. A need threshold marks the transition into '*Need To Defecate*', and an urgent threshold marks '*Urgent Need To Defecate*'. Each completed event increments a counter of defecations, and the internal state is reset, starting a new cycle. At each step, the update logic advances the state based on elapsed minutes since the last event. '*Just Defecated*' immediately becomes '*No Need To Defecate*' with the comfort level restored. While in '*No Need To Defecate*', the agent remains comfortable until the combined reach and keep times pass, then enters '*Building Pressure*'. In '*Building Pressure*', the comfort level decreases each step; crossing the need threshold moves the agent to '*Need To Defecate*'. There, comfort continues to decline and is clamped at the urgent threshold; once it reaches that point, the state becomes '*Urgent Need To Defecate*'. During satisfy, if the agent is not in a transport mode and is in '*Need To Defecate*' or '*Urgent Need To Defecate*', the agent acts to relieve the need, returning to '*Just Defecated*' and restarting the cycle.

Table 2. Summary of simulation parameters governing defecation, disease progression, and pathogen transmission

Parameter	Default Value	Description
Defecation rate bounds	$r_{\min} \in [0.2, 0.8]$ $r_{\max} \in [0.2, 0.8]$	Lower and upper bounds used to sample heterogeneous defecation rates.
Incubation period	$D_E = 3$ days	Duration an exposed agent waits before becoming infectious.
Infectious period	$D_I = 3$ days	Number of days an infectious agent sheds pathogens.
Recovery period	$D_R = 3$ days	Time until recovered agents return to susceptible state.
Infection ratio	$p_{\text{inf}} = 0.1$	Probability that a contact results in infection.
Spreading per person	$n_{\text{spread}} = 1$	Maximum agents an infectious individual may infect in one step.
Spreading per unit	$n_{\text{unit}} = 1$	Maximum agents that may become infected within a contaminated unit per agent.
Initial infected agents	1	Number of agents in infectious state at the start of the simulation.
Chance of infection	$U(0, 1)$	Individual-level susceptibility parameter.
Chance of spreading	$U(0, 1)$	Individual-level contagiousness parameter.
Shedding rate	$U(0, 1)$	Controls magnitude of pathogen shedding over time.

In addition, we separated the eating rate from the defecation rate to better reflect realistic physiological variation. Some individuals may eat large amounts but defecate only once, while others eat heavily and defecate frequently. Likewise, some people eat very little yet still defecate multiple times, and others eat little and rarely defecate. To capture this diversity, each agent is assigned a defecation rate r , drawn from a uniform distribution. This rate determines the timing of the entire physiological cycle. After defecation, an agent experiences a period with no urge to defecate lasting $60 - 30r$ minutes, followed by a comfortable period of $180 - 60r$ minutes during which internal pressure gradually increases. As time progresses, the agent's internal emptiness decreases at a rate proportional to $0.65r$. When this internal value drops below the threshold $30 + 20r$, the agent begins to feel the need to defecate, and when the value reaches zero the agent enters an urgent state. After defecation, the internal state resets and the cycle starts again.

4.2 Simulation Parameters

A set of behavioral and epidemiological parameters govern the agent-based simulation. The key parameters are summarized in Table 2, and additional narrative descriptions are provided below.

Defecation need parameters. Each agent is assigned a defecation rate drawn from a uniform distribution bounded by a lower and upper limit (r_{\min}, r_{\max}). This rate determines how quickly the agent transitions from *no need to defecate* to *urgent need to defecate*. After defecation, the fullness level is reset to its maximum and decreases over time based on the individualized rate. Once two internal thresholds are crossed, the agent moves sequentially through “building pressure”, “need to defecate”, and “urgent need to defecate” states. If defecation occurs while not in transport, pathogen shedding may take place within the current spatial unit. This design produces heterogeneous waste-generation behaviors that drive variability in pathogen deposition across the environment.

Disease progression parameters. Disease evolution follows a four-state progression: *susceptible*, *exposed*, *infectious*, and *recovered*. The duration of the exposed, infectious, and recovered states are determined by three parameters: incubation period (D_E), infectious period (D_I), and recovery period (D_R). Transition is time-dependent, and agents return to the susceptible state after the recovery period, modeling short-term immunity and allowing reinfection.

Infection transmission parameters. Transmission is probabilistic and controlled by three main parameters: the infection ratio (p_{inf}), the number of secondary infections that can be attempted by an infectious agent per step (n_{spread}), and the number of individuals potentially infected per contaminated spatial unit (n_{unit}). If an infectious agent defecates in a shared unit, the model attempts infection of a subset of nearby agents, enabling both direct human-to-human and indirect environment-mediated spread.

Pathogen shedding parameters. Infectious agents shed pathogens at a rate sampled from a uniform distribution in $[0, 1]$. The pathogen load is updated using a gamma-like shedding curve that increases early in the infectious period, peaks, and then declines during recovery. This supports temporal variation in environmental contamination and captures diverse shedding profiles.

4.3 Infectious Disease and Shedding Modeling

To integrate disease dynamics within the patterns-of-life simulation, we developed an agent-based infectious disease model that captures the key mechanisms of disease transmission and infection progression at individual agent level. The model prioritizes both efficiency and realism, allowing disease spread conditional on daily agent interactions rather than being dictated by predefined mathematical equations (e.g., ordinary differential equations in compartmental model). For each agent, the model tracks its disease status, which evolves over time according to contact events, probabilistic rules, and individual biological variability.

4.3.1 Agent-based SEIR Framework. In our simulation, we adapted the infectious disease dynamics concept of susceptible-exposed-infected-recovered (SEIR) and applied it at individual agent level, that each agent transits among four states, Susceptible (S), Exposed (E), Infectious (I), and Recovered (R):

$$S \rightarrow E \rightarrow I \rightarrow R \rightarrow S.$$

Such a design enables simulation of disease dynamics at an individual level, allowing for heterogeneity in infection progression and shedding over time within the simulated population. In our simulation, we consider a disease transmits through respiratory route and infected people sheds pathogen in feces. Agents in susceptible status may become exposed after contact with an other infectious agents during social interactions. After exposure, they enter a latent phase, “exposed”, in which they neither transmit the pathogen nor shed it through feces. After certain period, they transit to infectious, actively shedding the pathogen (through respiratory droplets and feces) and capable of spreading the disease. Finally, they recover and gain immunity which could last for months to years before returning to the susceptible status. This cyclic structure reflects the natural disease dynamics of agents over long-term simulations.

4.3.2 State Progression and Timing. The transmission of disease in the simulation follows a realistic, probabilistic process driven by direct agent interactions. At the start of the simulation, a predefined number of agents are initialized as infectious to seed the outbreak, while all others begin in the susceptible state. Agents in the *Susceptible* state behave normally and do not contribute to pathogen shedding. As the simulation progresses, when a susceptible agent encounters an infectious one, the simulation model evaluates whether transmission can occur based on a series of probabilistic checks that govern infection likelihood and spread capacity. To prevent uncontrolled outbreaks, each infectious agent is assigned a predefined infection limit that caps the number of individuals it can infect during its infectious period. If the agent has remaining capacity to transmit the disease, a random transmission probability is drawn from a uniform distribution to determine whether infection may occur. If this initial draw succeeds, the target (susceptible) agent

then performs its own infection probability test, also sampled from a uniform distribution. These probabilistic checks capture individual-level variability in both transmitting and contracting infection, reflecting real-world differences in immune response, behavior, and lifestyle. Finally, a global disease-specific infection rate is applied to determine whether transmission occurs. Infection takes place only when all these probabilistic conditions are satisfied, ensuring that disease spread remains both stochastic and biologically realistic.

Once an agent becomes exposed, it remains in the *Exposed* state for an individualized duration before transitioning to the *Infectious* state. During the exposure period, the agent continues to move and interact with others but cannot yet transmit the disease. Each agent's exposure duration is drawn from a global exposure threshold modulated by a smoothing factor that introduces slight variability across agents. After the exposure period ends, the agent becomes infectious and begins shedding pathogens into the system. This shedding activity contributes to the overall pathogen load in the simulated environment. After remaining infectious for its assigned period, the agent transitions to the *Recovered* state, during which it temporarily gains immunity. Once the recovery period is completed, the agent returns to the *Susceptible* state and can once again participate in future infection cycles. This cyclical process of infection, recovery, and susceptibility enables the simulation to capture realistic epidemic waves and long-term population dynamics.

4.3.3 Infection Layers of Interaction. Infection in the simulation can occur through three interconnected layers of interaction that jointly capture both spatial and social aspects of disease spread.

First, agents may infect others who are simply co-located in the same place, representing incidental contact driven by shared physical proximity. Second, agents who are co-located and actively attempting to expand their social networks can spread the infection to newly encountered individuals, capturing social-mixing behavior beyond familiar groups. Third, agents who are co-located, socially active, and interacting with close contacts such as friends, family members, or roommates can also transmit the disease while strengthening existing relationships.

Together, these three layers—(1) Co-location Transmission, (2) Contact-Based Transmission with Social Expansion, and (3) Contact-Based Transmission with Network Strengthening—form a multi-level framework for simulating infection spread that reflects the intertwined spatial and social dimensions of real-world disease transmission.

(1) Co-location Transmission. One mode of disease spread in the simulation is based on co-location. When an agent detects that one of its basic needs is unmet—such as the need for social interaction (love and belonging), food, shelter, or defecation—it becomes active and initiates movement to satisfy that need. During this process, a co-location transmission mechanism is activated. A predefined parameter specifies the maximum number of agents that can be infected by a single infectious agent within the same location, preventing uncontrolled spread. This mechanism ensures that disease transmission occurs primarily among agents who are physically co-located and actively interacting, rather than indiscriminately affecting all agents in the vicinity. As agents move to fulfill their needs, they may encounter and infect others nearby, generating realistic patterns of spatially localized transmission that reflect everyday human behavior and movement dynamics.

(2) Contact-Based Transmission with Social Expansion. Another mode of transmission focuses on social relationships between agents, modeling infection spread through interactions within social networks. This mechanism captures infection events that occur when agents engage in social activities aimed at expanding their social connections. Such interactions represent close-contact scenarios, including social gatherings, dining with friends at restaurants, or meeting new individuals through shared activities.

When multiple agents occupy the same location, an infectious agent does not attempt to infect everyone nearby—only those within close proximity are considered potential transmission targets. This approach produces a more realistic spread pattern by emphasizing that infection requires physical closeness; simply being in the same building or seeing another agent across the street does not lead to transmission. Additionally, the simulation incorporates randomness in social behavior, allowing agents to occasionally encounter and infect strangers outside their immediate social networks. This feature enables the pathogen to move beyond tightly clustered communities, capturing cross-group interactions and more accurately reflecting real-world patterns of disease transmission.

(3) *Contact-Based Transmission with Network Strengthening.* The third mode of transmission occurs when agents interact within their established social networks, reinforcing existing relationships with close contacts such as friends, family members, or roommates. In these interactions, infection can spread through repeated and prolonged contact, which reflects the higher transmission risk associated with close and frequent interactions in real-world settings. This layer represents stable, high-trust relationships where physical proximity and duration of contact are both elevated, making transmission more probable. By incorporating this mechanism, the simulation captures persistent infection chains within households and tight social circles, complementing the transient dynamics of social expansion and the incidental nature of co-location transmission.

4.3.4 Mathematical Representation. At the core of the infection mechanism is a probabilistic model that governs both transmission and state progression. When a susceptible agent encounters an infectious one, infection occurs only if multiple independent probability checks succeed:

$$u_1 < p_{\text{spread}}, \quad u_2 < p_{\text{infect}}, \quad u_3 < \rho, \quad \text{and } n_{\text{spread}} < N_{\text{max}},$$

where $u_1, u_2, u_3 \sim U(0, 1)$ are random values drawn from a uniform distribution, p_{spread} is the infectious agent's ability to transmit, p_{infect} is the susceptibility of the recipient, ρ is the global infection ratio, and N_{max} is the maximum number of infections allowed per source agent. Only when all four conditions hold does the susceptible agent become exposed.

Suppose that agent i can infect at most N_{max} other agents during its infectious period. For each meeting between an infectious source i and a susceptible recipient r , infection occurs according to a factored probability model:

$$\Pr(r \text{ becomes } E \mid i \text{ meets } r) = \mathbf{1}\{\text{spread count} < N_{\text{max}}\} \times p_{\text{spread}} \times p_{\text{infect}} \times \rho.$$

Here, p_{spread} represents the infectious agent's transmissibility, p_{infect} the susceptibility of the recipient, and ρ a global infection ratio that regulates the baseline transmissibility of the disease. Each contact event is independent, and a successful transmission moves r to the exposed state while recording i as the infection source.

Once infected, each agent a maintains individualized durations for the exposed, infectious, and recovered states: $\theta_E(a)$, $\theta_I(a)$, and $\theta_R(a)$. These values determine how long the agent remains in each state before transitioning. Let $d_E(a)$, $d_I(a)$, and $d_R(a)$ represent the elapsed time in each state. The state transitions follow:

$$E \rightarrow I \text{ if } d_E(a) \geq \theta_E(a), \quad I \rightarrow R \text{ if } d_I(a) \geq \theta_I(a), \quad R \rightarrow S \text{ if } d_R(a) \geq \theta_R(a).$$

When an agent reverts to S , all infection-related counters and identifiers are reset, ensuring that subsequent infections are treated as new and independent events.

Introducing Heterogeneity. To avoid synchronized state transitions and to better reflect real-world variability, we introduce heterogeneity through a smoothness parameter $s \in [0, 1]$ drawn from a uniform distribution $s \sim U(0, 1)$. This

Table 3. Key configuration parameters used in the simulation experiments

Parameter	Value	Description
numOfAgents	10,000	Total number of simulated agents.
numberOfDaysToBeExposed	7	Exposure period in days.
numberOfDaysToBeInfectious	14	Infectious period in days.
numberOfDaysToBeRecovered	2800	Recovery duration in days
numberOfSpreadPerPerson	50	Maximum Number of infection attempts per infectious individual.
numberOfSpreadPerUnit	10	Maximum Number of infection attempts per building unit per agent.
numberOfInitialInfectedAgents	10	Number of infected agents at simulation start.
infectionRatio	(0.1, 0.15, 0.2, 0.25)	Infection rates used for comparison.

parameter perturbs the base durations $\bar{\theta}_E$, $\bar{\theta}_I$, and $\bar{\theta}_R$, which represent the global durations for the exposed, infectious, and recovered states. The individualized durations for each agent are computed as:

$$\tilde{\theta} = \lceil \bar{\theta} + (0.5 - s)\bar{\theta} \rceil.$$

Here, $\bar{\theta}$ denotes the global base value and $\tilde{\theta}$ the agent-specific adjusted value. The randomization ensures that agents transition at different times, producing smoother epidemic curves and more realistic infection dynamics across the simulated population.

Pathogen Shedding Dynamics. Each infected agent generates and sheds pathogens after certain period of time after infection, which was assumed to be the period that agent is infectious in this simulation. The pathogen load shed over time was modeled using a gamma-like function that captures a typical rise-and-decay pattern. The number of pathogen shed at t days after the agent became infectious is:

$$N(t) = N_0 t^b e^{-at}. \quad (1)$$

where N_0 is the number of pathogen shed at the day agent became infectious, a is the rate and b is the shape parameters. We used typical parameters are $a = 2$, $k = 8$, and $N_0 = 10^7$ in this simulation.

Simulation Update Cycle. The infection model operates in a discrete-time manner, where each simulation tick represents one unit of simulated time (e.g., 5 minutes). During each tick, every agent independently updates its internal disease state and interacts with other agents, synchronizing biological processes with social behavior. Specifically, at each step, the agent increments the time spent in its current health state (d_E , d_I , or d_R), updates its pathogen load if it is in the infectious state, and evaluates transition conditions based on the corresponding thresholds θ_E , θ_I , and θ_R . This iterative process allows infection dynamics to evolve continuously and organically as agents move, meet, and change states throughout the simulation.

5 Results

In this section we present the environmental setup used for the simulation experiments along with the resulting outcomes of the simulation.

5.1 Environmental Setup and Simulation Configuration

All simulations were executed on a system equipped with an 11th Gen Intel(R) Core(TM) i5-1135G7 CPU @ 2.40 GHz running Fedora Linux 42 (Workstation Edition) with 16 GiB of RAM. The simulation environment is defined by more than 60 parameters; we presented the most relevant ones in **Table 3**. For this study, we conducted simulations with a population of 10,000 agents within the boundary of Fulton County in Georgia, USA. Each simulation covered approximately 348 simulation days (100,000 5-minute ticks) and required about 10 hours to complete. We used the software in [4] to run the simulation in parallel and process the output data.

5.2 Experimental Results

We evaluated the model using infection rates from 0.1 to 0.5 with increments of 0.025. The complete collection of results including videos and plots is available on GitHub. This paper presents four representative plots that demonstrate the key findings, while the full artifacts can be accessed online.

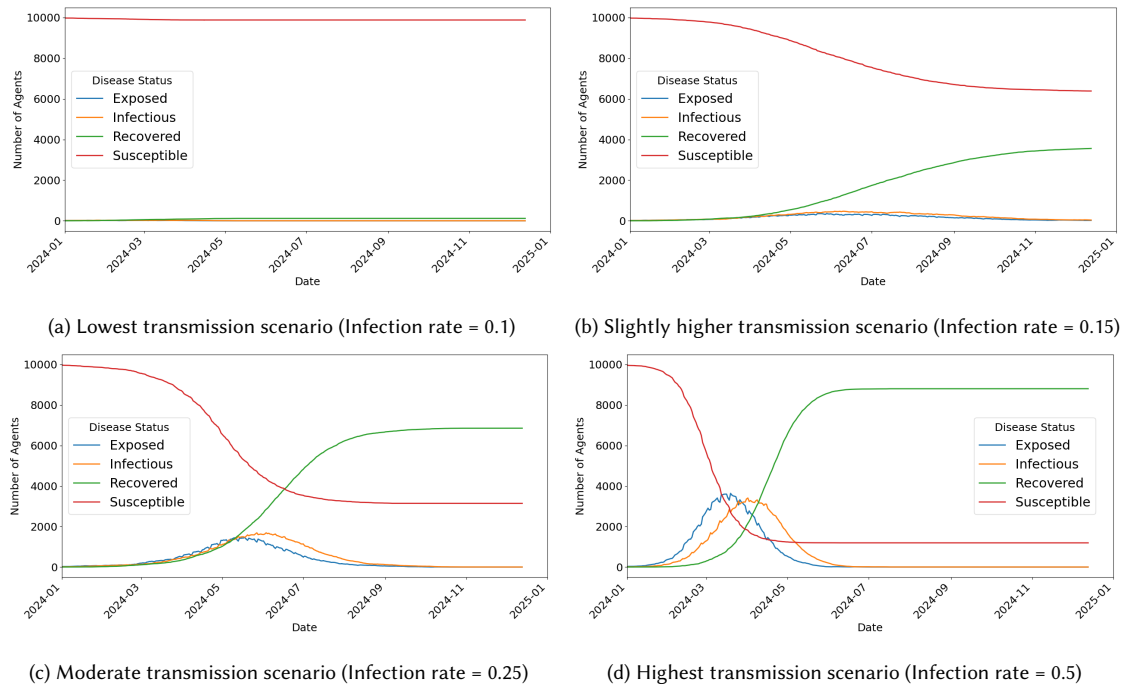


Fig. 3. Disease progression over time in the Fulton County 10K simulation across different infection rates. Full results for infection rates 0.1, 0.125, 0.15, 0.175, 0.2, up to 0.5 are available on GitHub.

5.2.1 Disease Dynamics. **Fig. 3** illustrates the temporal dynamics of disease progression for simulations conducted with varying infection rates (0.1, 0.15, 0.2, and 0.25) in a population of 10,000 agents in Fulton County. Each subplot depicts the transitions among key disease states—susceptible, exposed, infectious, and recovered. As infection rate increases, the spread accelerates, leading to higher and earlier peaks in the infectious population and a faster decline in susceptible individuals. This pattern highlights how elevated transmission rates intensify outbreak severity and shorten epidemic duration. Notably, we assume a long recovery period so individuals do not become susceptible again immediately. This prevents disease spread during recovery in the SEIR model, instead of allowing reinfection after

only a short recovery. **Fig. 3a:** In this scenario, only a small portion of the population transitions from susceptible to infected. The curves for exposed and infectious agents remain low throughout the simulation period, indicating limited disease spread. The susceptible population shows only a minimal decrease over time. As a result, recovered individuals constitute a very small fraction of the population by the end of the year. **Fig. 3b:** With an increased transmission rate, the epidemic expands more noticeably and reaches a higher peak of infectious individuals earlier in the year. The susceptible population gradually decreases as more individuals become exposed and later infectious. The recovered population grows steadily as immunity accumulates. Although the outbreak is more prominent than in the previous case, a substantial majority of agents remain susceptible by the end of the simulation. **Fig. 3c:** At this higher infection rate, the disease spreads rapidly through the population. The infectious and exposed curves rise sharply, reflecting a stronger and faster outbreak. The susceptible pool diminishes significantly as recovery rates increase and immunity becomes widespread. By the end of the year, the epidemic has affected a large portion of the population, leading to a dominant recovered group. **Fig. 3d:** Under aggressive transmission conditions, the epidemic unfolds very quickly. The susceptible population plummets early, as the infection spreads nearly unchecked through the community. Peaks in the exposed and infectious populations occur rapidly but are short lived due to the rapid exhaustion of susceptible agents. Eventually, the recovered population stabilizes at a very high level, indicating near complete epidemic saturation.

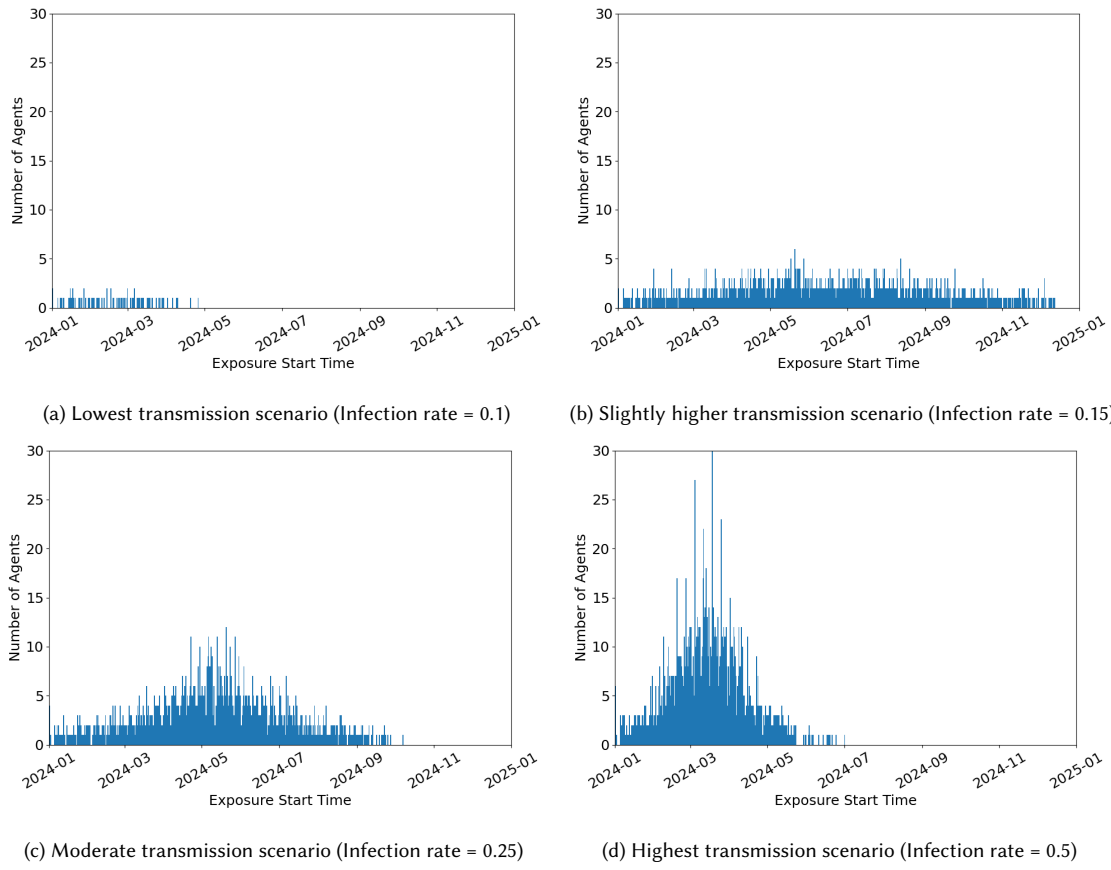


Fig. 4. Daily number of new cases in the Fulton County 10K simulation across different infection rates.

5.2.2 Epidemic Curve Analysis. **Fig. 4** presents the epidemic curves showing the daily number of new cases for simulations conducted with varying infection rates (0.1, 0.15, 0.25, and 0.5) in a population of 10,000 agents in Fulton County. Each subplot captures the temporal pattern of the outbreak for a specific infection probability, highlighting changes in peak intensity, outbreak duration, and overall epidemic behavior. As infection rates rise, the system transitions from minimal spread to rapid, high-intensity epidemic waves. These contrasts demonstrate the critical role of transmission probability in determining whether an outbreak remains contained or expands rapidly through the population. **Fig. 4a:** With an infection rate of 0.1, new case numbers remain consistently low throughout the simulation period. Transmission fails to build momentum, resulting in only small clusters of infections that fade quickly. The absence of any pronounced peak reflects insufficient spread to drive sustained epidemic growth. Most individuals remain uninfected, indicating an effectively self-limiting outbreak. **Fig. 4b:** At a transmission rate of 0.15, the outbreak becomes more evident and persists longer. Daily new cases rise gradually to a modest peak, showing that infections can propagate but still at limited speed. Although the epidemic is more sustained than in the lowest scenario, the number of newly infected agents remains relatively small, and transmission eventually subsides without overwhelming the population. **Fig. 4c:** With an infection rate of 0.25, the epidemic progresses much more aggressively. The case curve rises sharply, reaching a distinct peak as infections spread efficiently through the population. Following this rapid growth, daily case counts decline as susceptible individuals are depleted. This behavior is characteristic of a classical epidemic wave driven by strong transmission and expanding immunity. **Fig. 4d:** At the infection rate of 0.5, the outbreak escalates very quickly. New case counts surge early in the year, producing a short yet severe epidemic wave. Once susceptibility is exhausted, transmission collapses abruptly, and the epidemic ends rapidly. This scenario shows how high transmission induces intense but short-lived outbreaks due to rapid herd-immunity saturation. These comparisons confirm that increases in infection rate amplify the speed and magnitude of epidemic spread, producing earlier and sharper peaks while shortening the overall outbreak duration.

5.2.3 Temporal Variation in Pathogen Load. **Fig. 5** shows the total daily pathogen load in wastewater for simulations with varying infection rates (0.1, 0.15, 0.25, and 0.5) in a population of 10,000 agents in Fulton County. The temporal trends closely mirror the epidemic dynamics, since pathogen shedding depends on ongoing infections. As transmission increases, the wastewater signal becomes stronger, peaks earlier, and declines faster as susceptible individuals are depleted. This relationship highlights how wastewater-based surveillance provides a nonintrusive measure of outbreak scale and timing. **Fig. 5a:** With an infection rate of 0.1, pathogen levels in wastewater remain very low and fluctuate only briefly during the initial months. The signal disappears entirely by late spring, demonstrating that the outbreak is too small and short-lived to produce measurable contamination for an extended period. The data indicate minimal community spread and rapid failure of the pathogen to establish sustained transmission. **Fig. 5b:** At a transmission rate of 0.15, daily pathogen loads increase gradually as infections persist longer and occur in greater numbers. The peak remains moderate, but the presence of a clear curve extending into late summer reflects a more prolonged and noticeable outbreak. Although still controlled relative to higher transmission scenarios, the pathogen maintains environmental presence for much of the year. **Fig. 5c:** With an infection rate of 0.25, wastewater contamination increases sharply. Pathogen levels peak at high concentrations in late spring, matching the accelerated spread observed in disease dynamics. The signal then declines steadily as herd immunity builds and infection prevalence falls. This strong environmental signature is characteristic of a substantial and rapidly expanding epidemic wave. **Fig. 5d:** In the most aggressive transmission setting, pathogen loads escalate extremely fast and reach the highest values recorded among all simulations. The peak occurs early, followed by a rapid collapse once the susceptible pool is nearly exhausted.

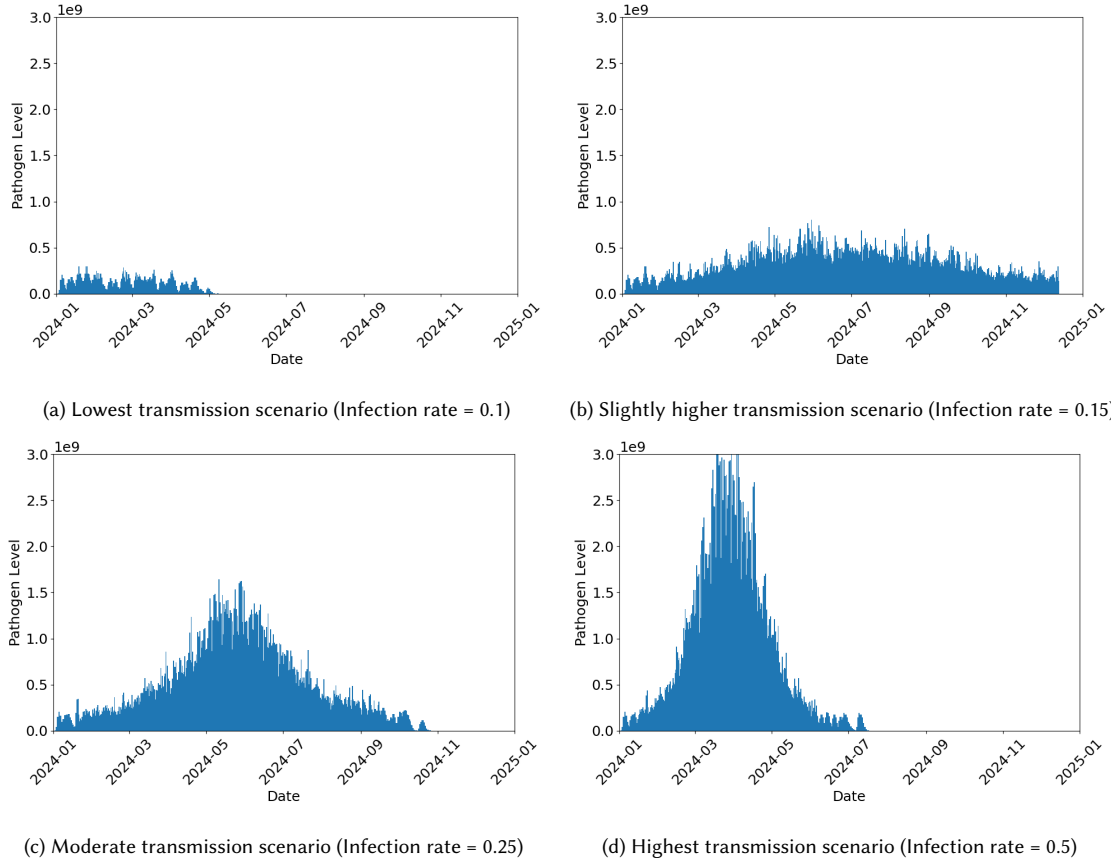


Fig. 5. Daily total pathogen load in wastewater for the Fulton County 10K simulation across different infection rates. Full results for infection rates 0.1, 0.125, 0.15, 0.175, 0.2, up to 0.5 are available on GitHub.

The brief but intense spike indicates widespread transmission compressed into a short period, making wastewater levels a highly sensitive and timely indicator of severe outbreaks. Overall, these results underscore that wastewater pathogen load serves as a robust indicator of epidemic scale, rising in tandem with infection prevalence and providing early warning of rapid outbreak growth.

5.2.4 Spatial Distribution of Pathogen Spread. **Fig. 6, Fig. 7, Fig. 8, and Fig. 9** illustrate the spatial progression of pathogen spread in the Fulton County 10K simulation on February 1, March 1, April 1, and May 1, 2024, respectively, across four infection rate scenarios (0.1, 0.15, 0.25, and 0.5). The maps demonstrate that higher transmission rates generate faster and more extensive spatial dissemination as the epidemic develops. Greater infection potential accelerates both the establishment of new shedding sites and their expansion across the county. As outbreaks intensify, the number of contaminated facilities increases and pathogen loads rise, resulting in stronger, denser, and more geographically connected spatial signatures over time. However, the highest infection rate triggers a much earlier and more intense outbreak, rapidly depleting the susceptible population. As a result, most individuals transition into the recovered state sooner, leaving fewer people available for new infections and greatly reducing pathogen contributions to the wastewater system in the later stages of the epidemic.

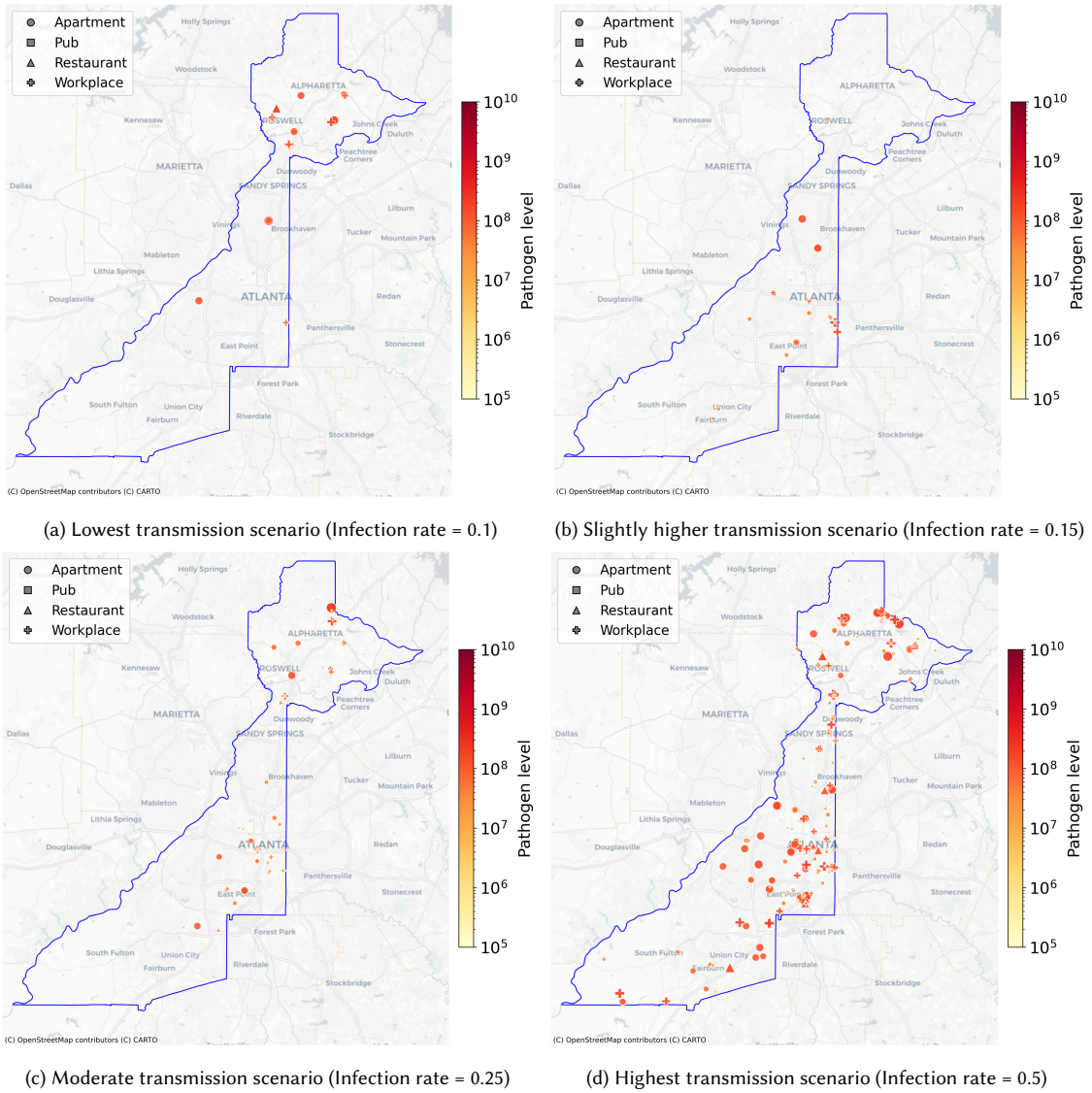


Fig. 6. Spatial distribution of pathogen spread in the Fulton County 10K simulation on February 1, 2024, across different infection rates. Full results for infection rates 0.1, 0.125, 0.15, 0.175, 0.2, up to 0.5 are available on GitHub.

Fig. 6 shows the spatial distribution of early outbreak activity on February 1, 2024, under four different infection rates. At this initial stage, pathogen shedding remains limited in all scenarios, but clear differences emerge based on transmission intensity. **Fig. 6a:** Only a few locations show low pathogen levels, indicating that transmission has not expanded significantly beyond initial introduction points. The magnitude of the pathogen load at each positive site appears high because it represents a per-agent shedding value defined in the simulation, which remains independent of the infection rate. **Fig. 6b:** A few additional shedding sites appear, increasing the total number of affected locations compared with the lowest transmission scenario. Spatial spread remains constrained, but early signs of community transmission begin to emerge. **Fig. 6c:** Multiple clusters are visible across northern and central Fulton County, indicating

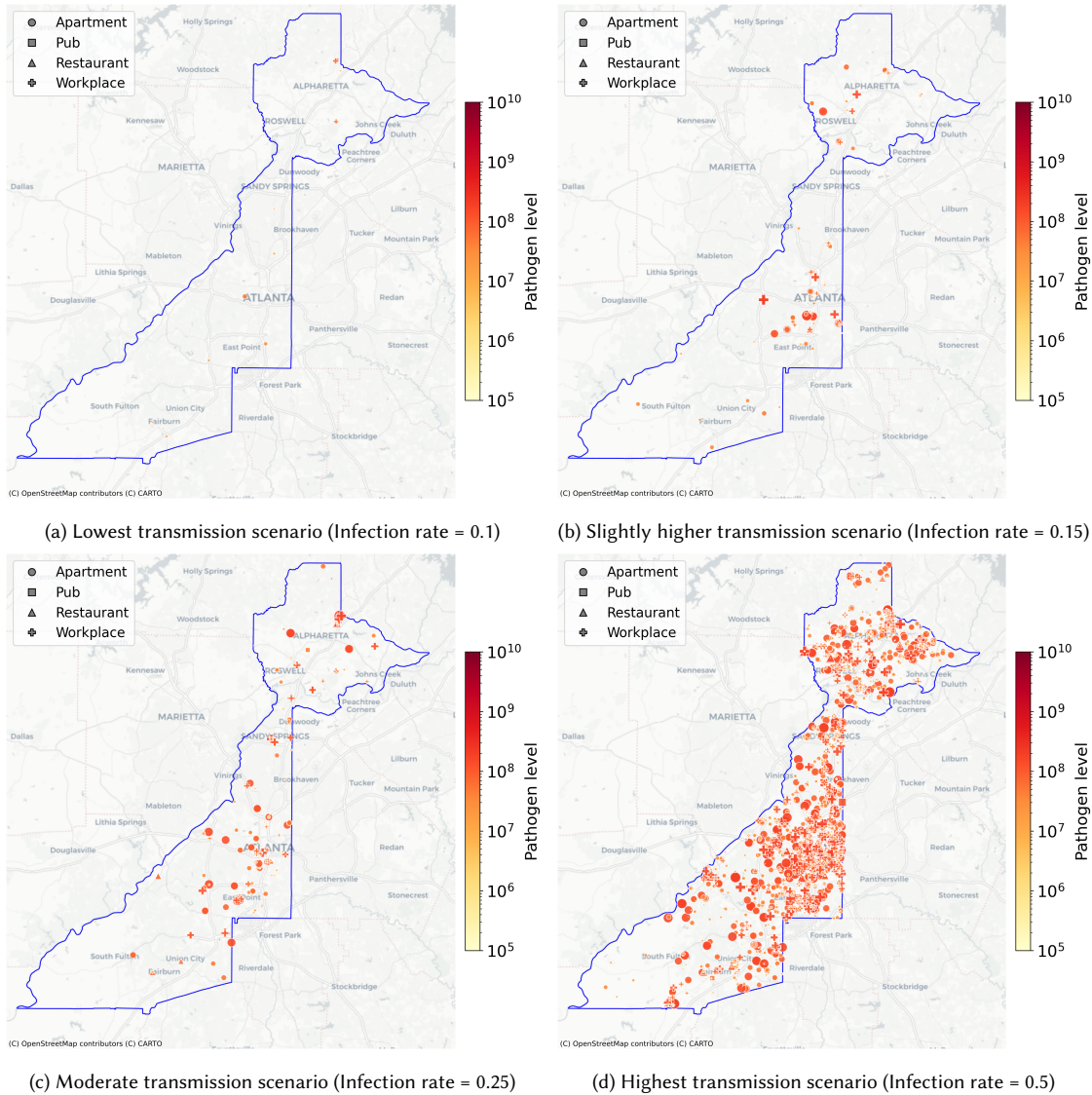


Fig. 7. Spatial distribution of pathogen spread in the Fulton County 10K simulation on March 1, 2024, across different infection rates. Full results for infection rates 0.1, 0.125, 0.15, 0.175, 0.2, up to 0.5 are available on GitHub.

stronger early propagation. Higher shedding intensity suggests that the outbreak is transitioning into sustained exponential growth. **Fig. 6d:** Large numbers of sites already exhibit substantial pathogen loads. Rapid, widespread seeding of infections has taken place across major residential and commercial areas, highlighting an aggressive early expansion of the epidemic.

Fig. 7 shows the spatial footprint of pathogen shedding one month later, on March 1, 2024. By this point, transmission differences between infection rate scenarios have become more pronounced, with higher rates producing broader and more intense contamination patterns across the county. **Fig. 7a:** Only a few scattered shedding sites remain

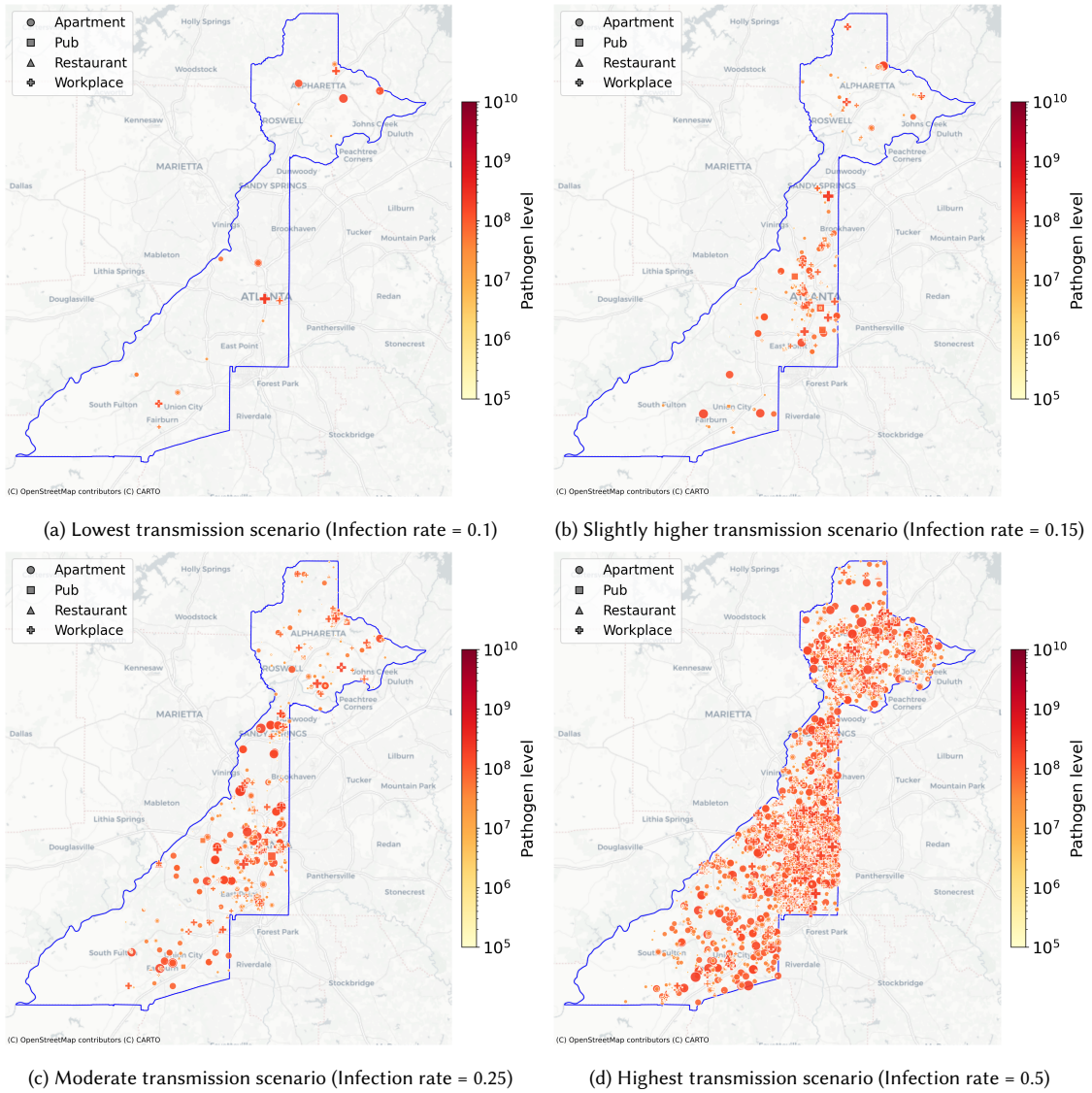


Fig. 8. Spatial distribution of pathogen spread in the Fulton County 10K simulation on April 1, 2024, across different infection rates. Full results for infection rates 0.1, 0.125, 0.15, 0.175, 0.2, up to 0.5 are available on GitHub.

detectable, all at low levels. Spatial propagation has largely stalled, indicating minimal community spread and a contained outbreak trajectory. **Fig. 7b**: Clusters of contamination emerge in central neighborhoods and along major mobility corridors. Although shedding remains moderate, infections are now persisting and expanding within connected social environments. **Fig. 7c**: Sheding becomes widespread, forming several high-intensity hotspots. The pathogen spreads efficiently across residential, commercial, and workplace settings, reflecting a rapidly growing epidemic with strong spatial connectivity. **Fig. 7d**: Nearly all populated regions exhibit high pathogen loads with dense clusters. This indicates extensive and mature community transmission, with few remaining unaffected areas across the county.

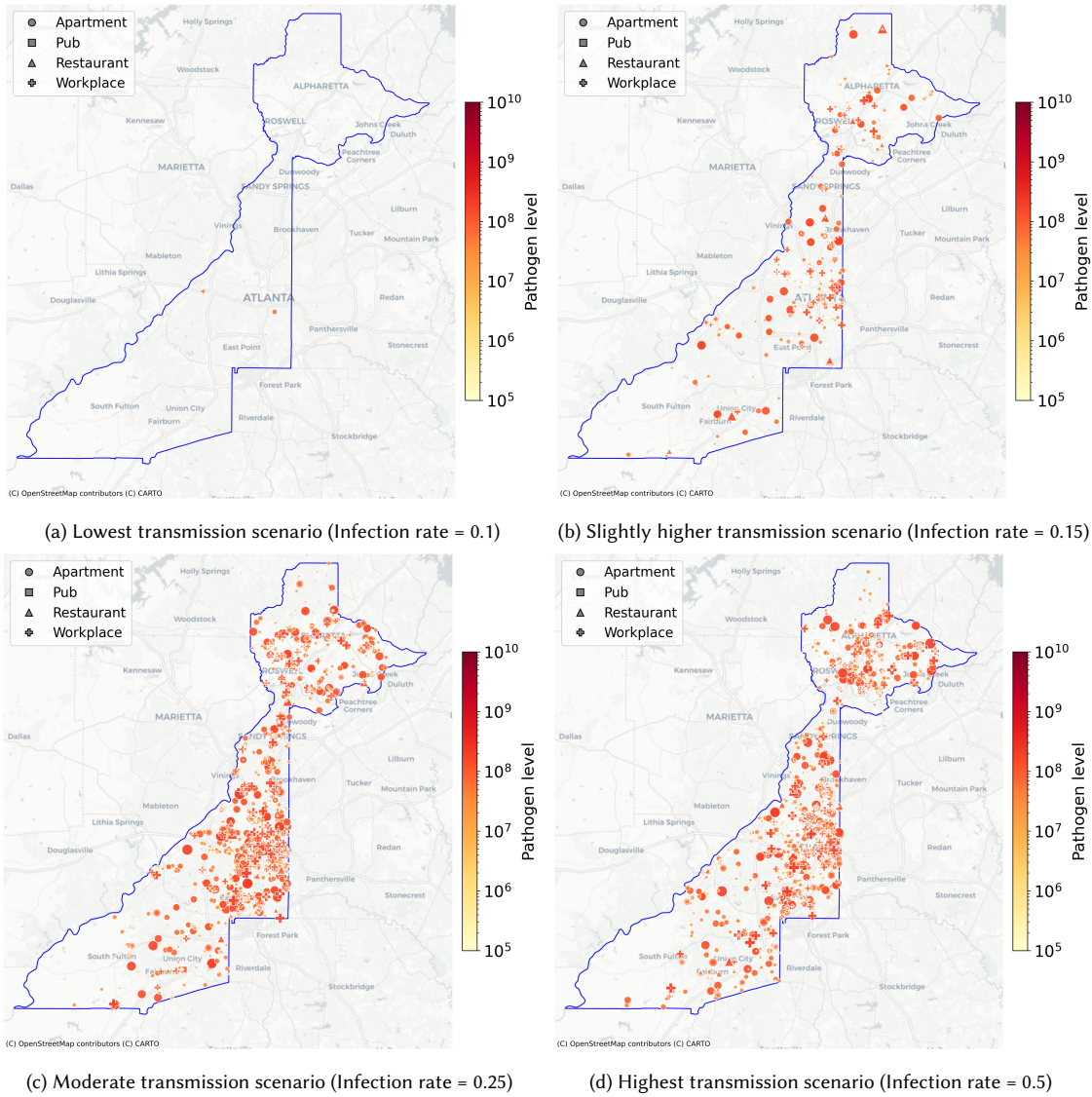


Fig. 9. Spatial distribution of pathogen spread in the Fulton County 10K simulation on May 1, 2024, across different infection rates. Full results for infection rates 0.1, 0.125, 0.15, 0.175, 0.2, up to 0.5 are available on GitHub.

Fig. 8 shows the spatial distribution of pathogen shedding on April 1, 2024, when transmission has progressed farther and spatial differences between scenarios are clearly established. Higher infection rates produce widespread clusters of contamination, while lower rates remain largely localized and constrained. **Fig. 8a:** Only a few low-intensity detections persist. Transmission remains highly limited, with no indication of significant expansion or sustained environmental contamination. **Fig. 8b:** Shedding becomes more spatially organized, forming multiple clusters around Atlanta and northern communities. Community spread is evident, though still moderate in scale. **Fig. 8c:** A large and continuous contaminated area emerges along the major population corridor. Many locations show strong shedding signals, demonstrating that the epidemic is now well established throughout the county. **Fig. 8d:** Widespread and

intense contamination covers nearly the entire region. High-shedding sites dominate both urban centers and suburban zones, indicating a fully developed outbreak with pervasive community transmission.

Fig. 9 shows the spatial extent of pathogen shedding on May 1, 2024. By this time, the epidemic has either remained localized or expanded dramatically depending on the infection rate. The resulting spatial patterns highlight the long-term consequences of different transmission intensities. **Fig. 9a:** Only a couple of isolated, low-intensity detections remain. The outbreak never achieves sustained transmission and is effectively extinguished. **Fig. 9b:** Shedding spreads further within clustered regions, primarily in central and northern parts of the county. Transmission continues, but the rate of spatial expansion remains relatively low. **Fig. 9c:** A large fraction of facilities show strong pathogen loads, reflecting widespread and ongoing community transmission supported by dense spatial connectivity. **Fig. 9d:** Shedding begins to decline as the susceptible population becomes exhausted and infected agents transition into the recovered state, where they can no longer be reinfected or contribute additional pathogen to the system.

6 Discussions

A major challenge in leveraging WBE for public health decision making lies in accurately defining the representativeness of WWS. This includes determining the proportion of infections detected (numerator) relative to the size of the population captured (denominator) and understanding the spatial distribution of the contributing population. Accurate catchment information is critical for normalizing wastewater measurements (i.e., transforming wastewater concentration to metrics that can be more comparable between samples), enabling timely interventions, and pinpointing target areas for public health action. While the WWS at downstream wastewater treatment facilities predominantly relies on sewer networks to define its catchment, the WWS catchment at the upstream site was more impacted by human behavior and social networks.

7 Conclusions

In this work, we presented an agent based geospatial simulation framework that links human behavior, infectious disease dynamics, and wastewater signals for wastewater based epidemiology. Building on the Patterns of Life simulation, we integrated daily mobility, multilayer social interactions, physiologically motivated defecation, and an individual level SEIR process with gamma like shedding dynamics. Using a case study of 10,000 agents in Fulton County, Georgia, we demonstrated how infection rates, mobility patterns, and toilet use jointly shape epidemic trajectories, wastewater pathogen loads, and the spatial spread of contamination.

Our results highlight three key insights for wastewater based epidemiology. First, mobility and toilet choice can substantially decouple residential population counts from wastewater contributions, especially at upstream sampling scales, explaining why nominal sewersheds populations can yield very different wastewater signals. Second, wastewater pathogen loads closely track epidemic timing and magnitude but can show nonlinear responses to changes in infection rate due to early depletion of susceptible individuals under high transmission. Third, spatial analyses reveal how shedding clusters emerge, merge, and dissipate over time, indicating transmission corridors and hotspots that are not visible in aggregated wastewater measurements alone.

This work also has limitations that motivate future research. The current implementation models only a single pathogen and a simplified SEIR structure, and does not include hydraulic transport or in sewer decay. Future extensions will incorporate realistic sewer flow, multiple pathogens, and behavior change in response to interventions. Calibration against empirical wastewater and case data will further refine model parameters and improve interpretability.

Overall, our findings show that behaviorally grounded agent based simulations can serve as a virtual laboratory for interpreting wastewater signals, evaluating surveillance system design, and exploring intervention scenarios. By explicitly connecting human movement, toilet use, and within host shedding to wastewater measurements, this framework supports improved design and analysis of wastewater based epidemiology in complex and dynamic urban environments.

8 Acknowledgment

This publication was made possible by the Insight Net cooperative agreement CDC-RFA-FT-23-0069 from the CDC's Center for Forecasting and Outbreak Analytics. Its contents are solely the responsibility of the authors and do not necessarily represent the official views of the Centers for Disease Control and Prevention. This research was also supported by the NSF #2109647.

References

- [1] Hossein Amiri, Will Kohn, Shiyang Ruan, Joon-Seok Kim, Hamdi Kavak, Andrew Crooks, Dieter Pfoser, Carola Wenk, and Andreas Züfle. 2024. The Patterns of Life Human Mobility Simulation. In *SIGSPATIAL '24*. 653–656.
- [2] Hossein Amiri, Ruochen Kong, and Andreas Züfle. 2024. Urban Anomalies: A Simulated Human Mobility Dataset with Injected Anomalies. In *Proceedings of the 1st ACM SIGSPATIAL International Workshop on Geospatial Anomaly Detection*. 1–11.
- [3] Hossein Amiri, Shiyang Ruan, et al. 2023. Massive Trajectory Data Based on Patterns of Life. In *SIGSPATIAL '23*. ACM, 1–4.
- [4] Hossein Amiri, Richard Yang, Shiyang Ruan, Joon-Seok Kim, Hamdi Kavak, Andrew Crooks, Dieter Pfoser, Carola Wenk, and Andreas Zufle. 2025. HD-GEN: A Software System for Large-Scale Human Mobility Data Generation Based on Patterns of Life. In *Proceedings of the 33rd ACM International Conference on Advances in Geographic Information Systems*. 407–410.
- [5] Chrystelle NH Atinkpahoun, Nang Dinh Le, Steve Pontvianne, Hélène Poirot, Jean-Pierre Leclerc, Marie-Noëlle Pons, and Henri H Soclo. 2018. Population mobility and urban wastewater dynamics. *Science of the Total Environment* 622 (2018), 1431–1437.
- [6] Jose Antonio Baz-Lomba, Francesco Di Ruscio, Arturo Amador, Malcolm Reid, and Kevin V Thomas. 2019. Assessing alternative population size proxies in a wastewater catchment area using mobile device data. *Environmental science & technology* 53, 4 (2019), 1994–2001.
- [7] Frederic Been, Luca Rossi, Christoph Ort, Serge Rudaz, Olivier Delémont, and Pierre Esseiva. 2014. Population normalization with ammonium in wastewater-based epidemiology: application to illicit drug monitoring. *Environmental science & technology* 48, 14 (2014), 8162–8169.
- [8] Tim Boogaerts, Maarten Quireyns, Hans De Loof, Xander Bertels, Natan Van Wichelen, Bram Pussig, Jan Saevels, Lies Lahousse, Pauline Bonmariage, Wouter Hamelinck, et al. 2023. Do the lockdown-imposed changes in a wastewater treatment plant catchment's socio-demographics impact longitudinal temporal trends in psychoactive pharmaceutical use? *Science of The Total Environment* 876 (2023), 162342.
- [9] Tim Boogaerts, Natan Van Wichelen, Maarten Quireyns, Dan Burgard, Lubertus Bijlsma, Peter Delputte, Celine Gys, Adrian Covaci, and Alexander LN van Nuijs. 2024. Current state and future perspectives on de facto population markers for normalization in wastewater-based epidemiology: A systematic literature review. *Science of The Total Environment* 935 (2024), 173223.
- [10] Néstor DelaPaz-Ruiz, P.W.M. Augustijn, Mahdi Farnaghi, [Shaheen A.] Abdulkareem, and R. Zurita-Milla. 2025. Integrating agent-based disease, mobility and wastewater models for the study of the spread of communicable diseases. *Geospatial health* 20, 1 (23 Jan. 2025). doi:10.4081/gh.2025.1326
- [11] Kata Farkas, Rachel Williams, Natasha Alex-Sanders, Jasmine MS Grimsley, Igor Pânteia, Matthew J Wade, Nick Woodhall, and Davey L Jones. 2023. Wastewater-based monitoring of SARS-CoV-2 at UK airports and its potential role in international public health surveillance. *PLOS global public health* 3, 1 (2023), e0001346.
- [12] Cynthia Gibas, Kevin Lambirth, Neha Mittal, Md Ariful Islam Juel, Visva Bharati Barua, Lauren Roppolo Brazell, Keshawn Hinton, Jordan Lontai, Nicholas Stark, Isaiah Young, et al. 2021. Implementing building-level SARS-CoV-2 wastewater surveillance on a university campus. *Science of The Total Environment* 782 (2021), 146749.
- [13] Joanne Hewitt, Sam Trowsdale, Bridget A Armstrong, Joanne R Chapman, Kirsten M Carter, Dawn M Croucher, Cassandra R Trent, Rosemary E Sim, and Brent J Gilpin. 2022. Sensitivity of wastewater-based epidemiology for detection of SARS-CoV-2 RNA in a low prevalence setting. *Water Research* 211 (2022), 118032.
- [14] Loren Hopkins, Katherine B Ensor, Lauren Stadler, Catherine D Johnson, Rebecca Schneider, Kaavya Domakonda, James J McCarthy, Edward J Septimus, David Persse, and Stephen L Williams. 2023. Public health interventions guided by Houston's wastewater surveillance program during the COVID-19 pandemic. *Public Health Reports* 138, 6 (2023), 856–861.
- [15] Loren Hopkins, David Persse, Kelsey Caton, Katherine Ensor, Rebecca Schneider, Camille McCall, and Lauren B Stadler. 2023. Citywide wastewater SARS-CoV-2 levels strongly correlated with multiple disease surveillance indicators and outcomes over three COVID-19 waves. *Science of The Total Environment* 855 (2023), 158967.

[16] Joon-Seok Kim, Hyunjee Jin, Hamdi Kavak, et al. 2020. Location-based social network data generation based on patterns of life. In *MDM*. IEEE, 158–167.

[17] Will Kohn, Hossein Amiri, and Andreas Züfle. 2023. EPIPOL: An Epidemiological Patterns of Life Simulation (Demonstration Paper). In *SIGSPATIAL SpatialEpi'23 Workshop*. ACM, 13–16.

[18] Kang Mao, Kuankuan Zhang, Wei Du, Waqar Ali, Xinbin Feng, and Hua Zhang. 2020. The potential of wastewater-based epidemiology as surveillance and early warning of infectious disease outbreaks. *Current opinion in environmental science & health* 17 (2020), 1–7.

[19] Abraham H Maslow. 1943. A theory of human motivation. *Psychological review* 50, 4 (1943), 370.

[20] Gertjan Medema, Frederic Been, Leo Heijnen, and Susan Petterson. 2020. Implementation of environmental surveillance for SARS-CoV-2 virus to support public health decisions: opportunities and challenges. *Current opinion in environmental science & health* 17 (2020), 49–71.

[21] Nicolas Neuenhofer, Andy Disch, Stephan Baumgartner, Christoph Ort, and Jörg Rieckermann. 2025. Exploring the relationship between mobile positioning data and wastewater flows: evidence from five Swiss catchments. *Water Science & Technology* 92, 5 (2025), 669–682.

[22] Sizwe Nkambule, Renée Street, Swastika Surujal-Naicker, Rabia Johnson, and Angela Mathee. 2024. Wastewater surveillance for SARS-CoV-2 during a mass sporting event in the City of Cape Town, Western Cape. *Frontiers in Public Health* 12 (2024), 1462629.

[23] Christoph Ort, Michael G Lawrence, Jorg Rieckermann, and Adriano Joss. 2010. Sampling for pharmaceuticals and personal care products (PPCPs) and illicit drugs in wastewater systems: are your conclusions valid? A critical review. *Environmental science & technology* 44, 16 (2010), 6024–6035.

[24] John R Paul and JAMES D TRASK. 1941. The virus of poliomyelitis in stools and sewage. *Journal of the American Medical Association* 116, 6 (1941), 493–498.

[25] David Polo, Marcos Quintela-Baluja, Alexander Corbishley, Davey L Jones, Andrew C Singer, David W Graham, and Jesús L Romalde. 2020. Making waves: wastewater-based epidemiology for COVID-19—approaches and challenges for surveillance and prediction. *Water research* 186 (2020), 116404.

[26] Mackay Price, Ben Tscharke, Andrew Chappell, Melanie Kah, Katarzyna Sila-Nowicka, Helen Morris, Daniel Ward, and Sam Trowsdale. 2024. Testing methods to estimate population size for wastewater treatment plants using census data: implications for wastewater-based epidemiology. *Science of The Total Environment* 922 (2024), 170974.

[27] AJ Rhodes, Eina M Clark, Dorothy S Knowles, FRANK SHIMADA, Alice M Goodfellow, RC Ritchie, and WL Donohue. 1950. Poliomyelitis virus in urban sewage: an examination for its presence over a period of twelve months. *Canadian Journal of Public Health/Revue Canadienne de Santé Publique* 41, 6 (1950), 248–254.

[28] Lindsay B Saber, Shanika S Kennedy, Yixin Yang, Kyler N Moore, Yuke Wang, Stephen P Hilton, Tylis Y Chang, Pengbo Liu, Victoria L Phillips, Matthew J Akiyama, et al. 2024. Correlation of SARS-CoV-2 in wastewater and individual testing results in a jail, Atlanta, Georgia, USA. *Emerging Infectious Diseases* 30, Suppl 1 (2024), S21.

[29] Nina Schmid, Julia Bicker, Andreas F Hofmann, Karina Wallrafen-Sam, David Kerkmann, Andreas Wieser, Martin J Kühn, and Jan Hasenauer. 2025. Integrative modeling of the spread of serious infectious diseases and corresponding wastewater dynamics. *Epidemics* (2025), 100836.

[30] Laura C Scott, Alexandra Aubeel, Layla Babahaji, Katie Vigil, Scott Tims, and Tiong Gim Aw. 2021. Targeted wastewater surveillance of SARS-CoV-2 on a university campus for COVID-19 outbreak detection and mitigation. *Environmental research* 200 (2021), 111374.

[31] Wonjin Sim, Suyeon Park, Jihye Ha, Donghyun Kim, and Jeong-Eun Oh. 2023. Evaluation of population estimation methods for wastewater-based epidemiology in a metropolitan city. *Science of The Total Environment* 857 (2023), 159154.

[32] Natalie Sims and Barbara Kasprowy-Hordern. 2020. Future perspectives of wastewater-based epidemiology: monitoring infectious disease spread and resistance to the community level. *Environment international* 139 (2020), 105689.

[33] Kevin V Thomas, Arturo Amador, Jose Antonio Baz-Lomba, and Malcolm Reid. 2017. Use of mobile device data to better estimate dynamic population size for wastewater-based epidemiology. *Environmental science & technology* 51, 19 (2017), 11363–11370.

[34] Janelle R Thompson, Yarlagadda V Nanchariah, Xiaoqiong Gu, Wei Lin Lee, Verónica B Rajal, Monamie B Haines, Rosina Girones, Lee Ching Ng, Eric J Alm, and Stefan Wuertz. 2020. Making waves: wastewater surveillance of SARS-CoV-2 for population-based health management. *Water research* 184 (2020), 116181.

[35] James D Trask, John R Paul, et al. 1942. Periodic examination of sewage for the virus of poliomyelitis. *The Journal of Experimental Medicine* 75, 1 (1942), 1.

[36] Benjamin J Tscharke, Jake W O'Brien, Christoph Ort, Sharon Grant, Cobus Gerber, Richard Bade, Phong K Thai, Kevin V Thomas, and Jochen F Mueller. 2019. Harnessing the power of the census: characterizing wastewater treatment plant catchment populations for wastewater-based epidemiology. *Environmental science & technology* 53, 17 (2019), 10303–10311.

[37] Matthew J Wade, Anna Lo Jacomo, Elena Armenise, Mathew R Brown, Joshua T Bunce, Graeme J Cameron, Zhou Fang, Deidre F Gilpin, David W Graham, Jasmine MS Grimsley, et al. 2022. Understanding and managing uncertainty and variability for wastewater monitoring beyond the pandemic: lessons learned from the United Kingdom national COVID-19 surveillance programmes. *Journal of hazardous materials* 424 (2022), 127456.

[38] Yuke Wang, Pengbo Liu, Jamie VanTassell, Stephen P Hilton, Liheng Guo, Orlando Sablon, Marlene Wolfe, Lorenzo Freeman, Wayne Rose, Carl Holt, et al. 2023. When case reporting becomes untenable: Can sewer networks tell us where COVID-19 transmission occurs? *Water research* 229 (2023), 119516.

[39] Yuke Wang, Pengbo Liu, Haisu Zhang, Makoto Ibaraki, Jamie VanTassell, Kelly Geith, Matthew Cavallo, Rebecca Kann, Lindsay Saber, Colleen S Kraft, et al. 2022. Early warning of a COVID-19 surge on a university campus based on wastewater surveillance for SARS-CoV-2 at residence halls. *Science of The Total Environment* 821 (2022), 153291.

- [40] Zheng Zhang, Hossein Amiri, Zhenke Liu, Liang Zhao, and Andreas Züfle. 2024. Large language models for spatial trajectory patterns mining. In *Proceedings of the 1st ACM SIGSPATIAL International Workshop on Geospatial Anomaly Detection*. 52–55.
- [41] Zheng Zhang, Hossein Amiri, Dazhou Yu, Yuntong Hu, Liang Zhao, and Andreas Züfle. 2024. Transferable Unsupervised Outlier Detection Framework for Human Semantic Trajectories. In *SIGSPATIAL’24*. 350–360.
- [42] Andreas Züfle, Carola Wenk, Dieter Pfoser, Andrew Crooks, Joon-Seok Kim, Hamdi Kavak, Umar Manzoor, and Hyunjee Jin. 2023. Urban life: a model of people and places. *Computational and Mathematical Organization Theory* 29, 1 (2023), 20–51.